Ceramics International xxx (xxxx) xxx

Contents lists available at ScienceDirect

Ceramics International

journal homepage: www.elsevier.com/locate/ceramint

Short communication

A new high-$Q\times f$ Li_4NbO_4F microwave dielectric ceramic for LTCC applications

Xin Chu, Juan Jiang, Jinzhao Wang, Yuanchuang Wu, Lin Gan *, Tianjin Zhang **

Hubei Collaborative Innovation Center for Advanced Organic Chemical Materials, Ministry of Education Key Laboratory for the Green Preparation and Application of Functional Materials and School of Material Science and Engineering, Hubei University, Wuhan, 430062, China

ARTICLE INFO

Keywords:
Rock salt
Microwave dielectric properties
LTCC

ABSTRACT

A novel microwave dielectric ceramic material, Li_4NbO_4F, was fabricated by the solid-state reaction method. The microwave dielectric properties, sintering characteristics, and crystal structures of the Li_4NbO_4F ceramic samples were investigated. It was found that the Li_4NbO_4F ceramic samples can be successfully sintered at low temperatures (e.g., 750–875 °C). The samples exhibited a single cubic rock salt phase and possessed homogenous microstructures and outstanding microwave dielectric properties. The optimal properties of $Q \times f = 61111$ GHz, $\varepsilon_r = 15.2$, and $\tau_f = -51$ ppm/°C were achieved in the ceramic sample sintered at 825 °C. Additionally, the ceramic samples showed superior compatibility with Ag, indicating that Li_4NbO_4F is a promising low-temperature co-fired ceramic (LTCC) material.

1. Introduction

In recent years, the prevalence of the fifth generation mobile networks and the Internet of Things, as a part of the rapid development of mobile communications, has aroused considerable interest in the exploration of high-performance microwave dielectric ceramic materials (MDCMs) [1]. It is known that low-temperature co-fired ceramic (LTCC) materials possess outstanding microwave dielectric properties (MDPs), have a low sintering temperature (≤950 °C), and exhibit excellent chemical compatibility with Ag electrodes [2]. This makes them key components of various electronic devices such as resonators, filters, oscillators, and antenna substrates [3,4]. Generally, for their applications in substrates for patch antennas, LTCC materials are necessary to possess a high quality factor ($Q \times f$) and a low dielectric constant (ε_r). In addition, a near-zero temperature coefficient of resonant frequency (τ_f) is also favorable for enhancing the temperature stability of devices [5].

In order to achieve the low sintering temperature below the melting point of silver (961 °C), sintering additives such as $BaCu(B_2O_5)$, Li_2CO_3, H_3BO_3, or low-melting glassy materials are typically employed to lower the sintering temperature [6–9]. Alternatively, some additive-free ceramics with low sintering temperature were successfully exploited in recent decades [10,11]. However, it is widely known that the use of improper sintering aids or high amount additions will, without exception, decrease the $Q \times f$ values due to the formation of undesirable intergranular glass or impurity phases [12]. Therefore, it is necessary to develop novel high-$Q \times f$ LTCC materials without the requirement of additives. Li-containing ceramics with a rock salt structure, which mainly include $LiFeO_2$, Li_2ZrO_3, Li_2TiO_3, $Li_2Mg_3TiO_6$, and $Li_3Mg_2NbO_6$, reportedly have low ε_r (e.g., <20) as well as high $Q \times f$ levels (e.g., >50000 GHz) [13]. Nevertheless, their application as LTCC materials is considerably hindered because they usually require relatively high sintering temperatures (~1200 °C) [14–16]. Recently, it was found that the partial replacement of O^{2-} by F^- can facilitate a remarkable decrease in the sintering temperature of the rock salt-structured materials. Zhang et al. [17] reported that $Li_5Ti_2O_6F$ ceramics with a cubic rock salt structure, when sintered at 880 °C, showed superior MDPs ($Q \times f =$ 79500 GHz, $\varepsilon_r = 19.6$, and $\tau_f = -29.6$ ppm/°C). Subsequently, the same team developed another rock-salt-structured ceramic material of $Li_7Ti_3O_9F$ at 950 °C, having $Q \times f = 88200$ GHz, $\varepsilon_r = 22.5$, and $\tau_f = -24.2$ ppm/°C [18]. Zhang et al. [19] successfully decreased the sintering temperature of $Li_2Mg_3TiO_6$ from 1280 to 950 °C by partial replacement of O^{2-} by F^- (e.g., 8 at.%).

In this work, the authors attempted to fabricate a Li_4NbO_4F ceramic using the solid-state reaction method. The MDPs, sintering behavior, and crystal structures of the Li_4NbO_4F ceramic samples were

* Corresponding author.
** Corresponding author.
E-mail address: ganlin@hubu.edu.cn (L. Gan).

https://doi.org/10.1016/j.ceramint.2020.09.280
Received 22 August 2020; Received in revised form 28 September 2020; Accepted 30 September 2020
Available online 1 October 2020

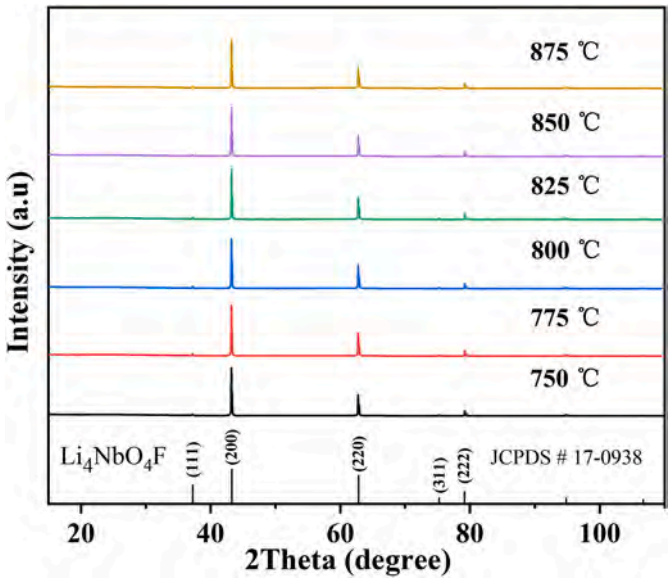

Fig. 1. XRD patterns of Li_4NbO_4F samples sintered at various temperatures.

investigated in detail. The specimens presented both low sintering temperatures and high $Q \times f$ levels. In addition, the chemical compatibility of Li_4NbO_4F ceramics with silver electrodes was also found to be excellent.

2. Experimental procedure

Li_4NbO_4F specimens were prepared by the solid-state reaction method using powders of Li_2CO_3 (98.9%, Sinopharm, China), LiF (99.9%, Sinopharm, China), and Nb_2O_5 (99.9%, Zibo Weijie, China). Initially, Li_2CO_3, LiF, and Nb_2O_5 were weighed and mixed in ethanol (98%, Alladin, China) for 8 h with ZrO_2 balls. After drying at 90 °C, the powder was heated at 700 °C for 4 h to obtain Li_4NbO_4F. The as-obtained powder was ball milled and dried again, then the powder was mixed with polyvinyl alcohol (5 wt%). The green bodies were dry-pressed at 4 MPa (Φ = 14 mm, 6–7 mm high). Eventually, the samples were debindered at 540 °C for 2 h and sintered at different temperatures for 2 h (i.e., 750–875 °C).

The phases and crystal structures of the ceramics were analyzed by X-ray powder diffraction (XRD, D 2500, Rigaku, Japan). The density of the

Table 1
Calculated structural parameters and corresponding reliability factors of Li_4NbO_4F ceramics sintered at various temperatures.

Sintering temperature (°C)	a = b = c (Å)	α = β = γ (°)	V(Å^3)	*Rp*	*Rwp*	x^2
750 °C	4.18689	90	73.396 (0.004)	2.34	3.11	1.73
775 °C	4.18742	90	73.424 (0.004)	2.94	3.91	1.44
800 °C	4.18756	90	73.432 (0.004)	2.24	2.94	1.58
825 °C	4.18783	90	73.446 (0.000)	3.05	3.97	1.42
850 °C	4.18885	90	73.499 (0.004)	3.11	4.09	1.49
875 °C	4.18860	90	73.486 (0.004)	2.31	3.05	1.66

Table 2
Refined atomic coordination parameters of the Li_4NbO_4F ceramic sample sintered at 825 °C.

T = 825 °C	Wyck. Site	Site sym.	X	Y	Z
Li	4a	m-3m	0	0	0
F	4b	m-3m	0.5	0.5	0.5
O	4b	m-3m	0.5	0.5	0.5
Nb	4a	m-3m	0	0	0

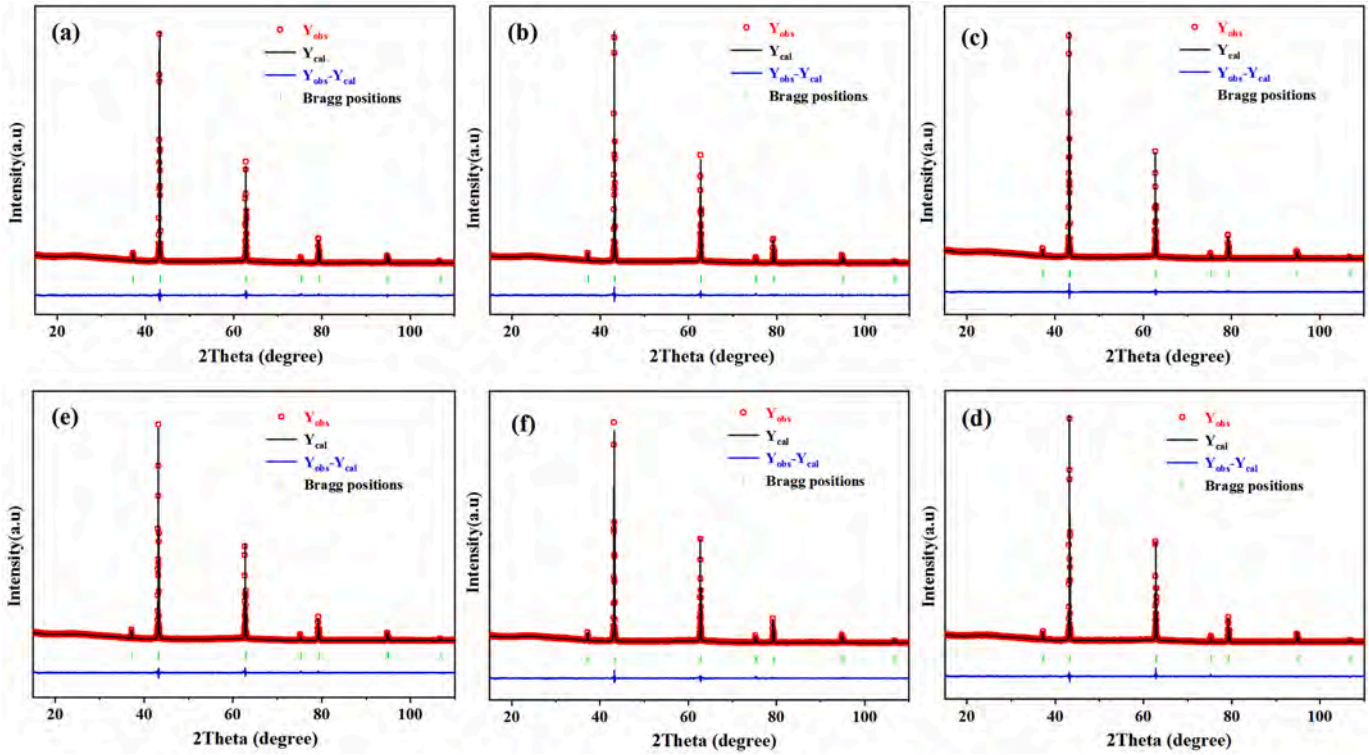

Fig. 2. Refined XRD patterns of Li_4NbO_4F ceramics sintered at various temperatures of (a) 750, (b) 775, (c) 800, (d) 825, (e) 850, and (f) 875 °C.

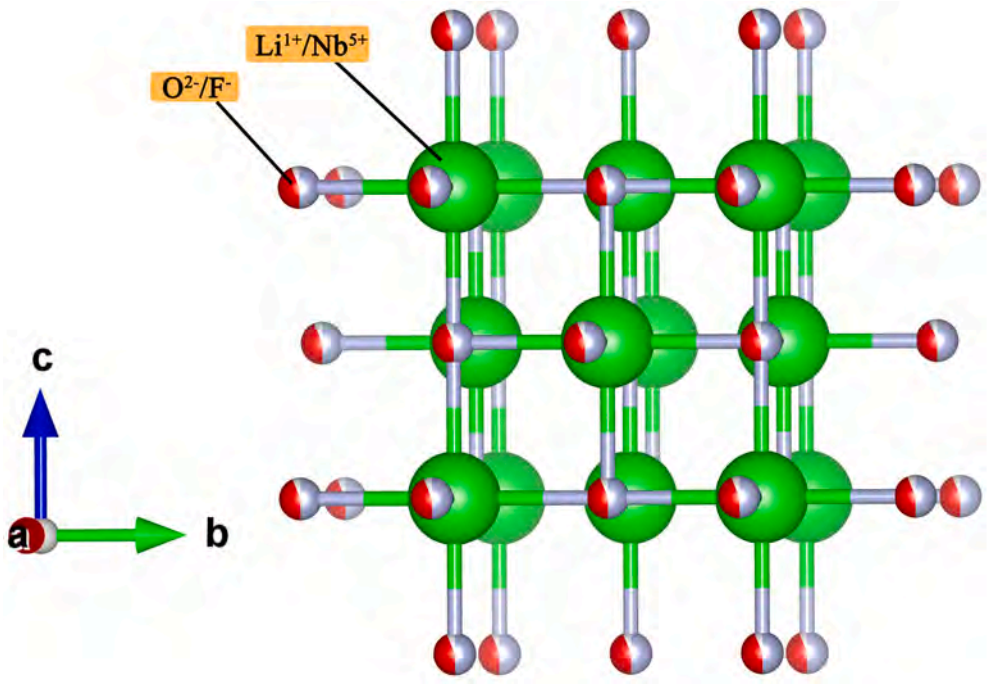

Fig. 3. Cubic rock salt structure of Li_4NbO_4F; the small and large balls represent O^{2-}/F^{-} ions and Li^{1+}/Nb^{5+} ions, respectively.

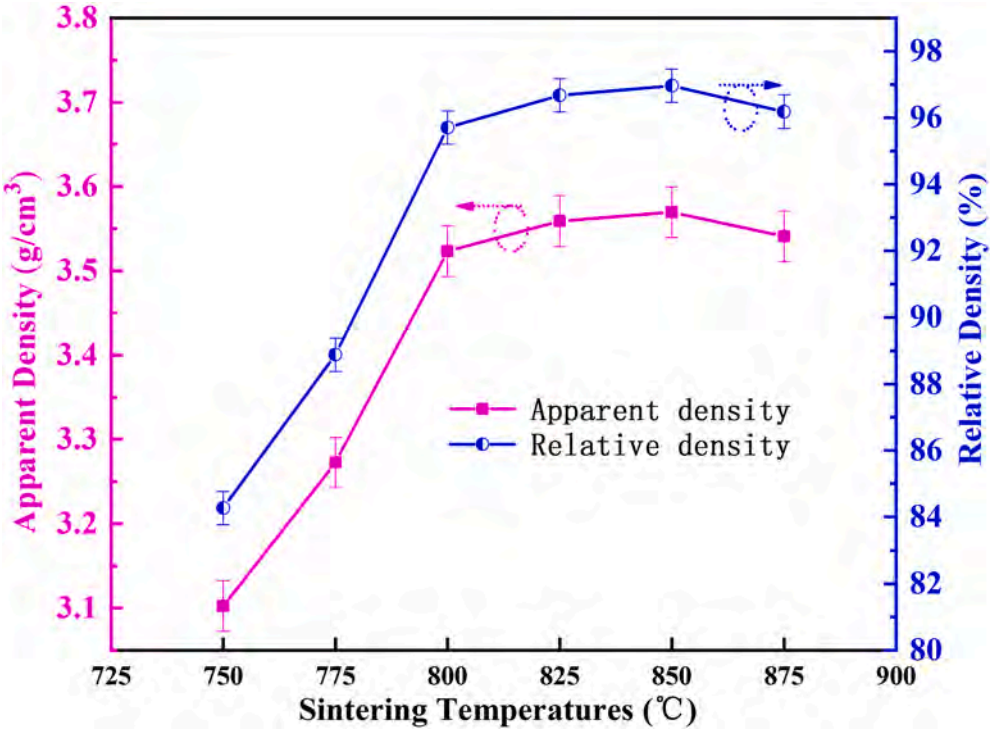

Fig. 4. Apparent density and relative density of Li_4NbO_4F specimens sintered at various temperatures.

specimens was determined using the Archimedes method. Microstructural and compositional analyses were conducted through scanning electron microscopy (SEM, JSM 6510LV, JEOL Japan) with energy dispersive spectrometry (EDS, Aztec, Oxford, UK). Before SEM observations, the ceramics were polished and thermally etched. Raman spectroscopy was carried out on a Raman spectrometer (Labram, Horiba, Japan). The MDPs of the Li_4NbO_4F ceramic specimens were measured using a network analyzer (E5071, Agilent, USA) in the TE_{011} mode. The Hakki–Coleman method was used to measure the ε_r and $Q \times f$ values. τ_f was calculated using the following equation:

$$\tau_f = \frac{f_1 - f_2}{f_1(T_2 - T_1)}, \quad (1)$$

where f_1 and f_2 are the resonant frequencies at 20 (T_1) and 85 (T_2)°C, respectively.

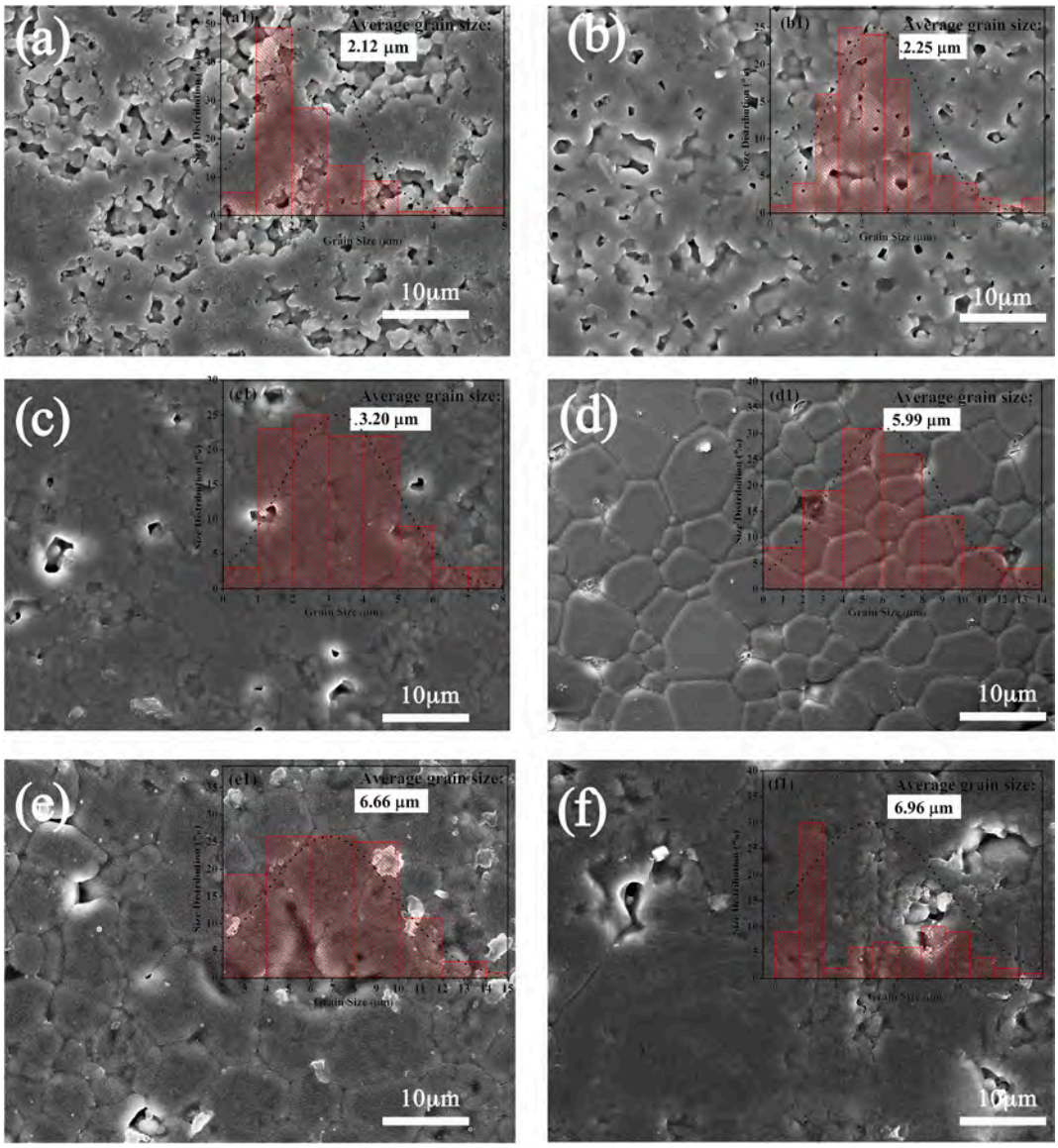

Fig. 5. SEM images of Li_4NbO_4F samples sintered at various temperatures of (a) 750, (b) 775, (c) 800, (d) 825, (e) 850, and (f) 875 °C; the insets show the grain size distribution and average grain size of each sample.

3. Results and discussion

Fig. 1 shows the XRD results of the Li_4NbO_4F samples sintered at different temperatures. All peaks were indexed to a cubic rock salt phase (Fm-3m) (JCPDS#17–0938), and no impurity phase were observed in any of the samples. Rietveld refinement was performed based on the XRD results for further analyses of the crystal structure and relative density.

Fig. 2 presents the refined XRD plots of the specimens sintered at various temperatures. The black line and red circles represent the calculated and experimental profiles, respectively. The bottom blue line shows the deviation between the calculated and observed intensities. The vertical bars below the patterns indicate the peak positions. Based on these refinement results, the structural characteristics of the ceramic specimens were calculated. Table 1 lists the lattice parameters, unit cell volumes, and reliability factors (i.e., *Rp*, *Rwp*, and x^2) of the Li_4NbO_4F specimens. In general, as the sintering temperature increased, the lattice parameters and cell volume of the Li_4NbO_4F ceramics slightly increased.

Table 2 summarizes the refined atomic coordinates of the rock-salt-structured Li_4NbO_4F. Based on the results, a schematic diagram of a unit cell of Li_4NbO_4F with a rock salt structure is shown in Fig. 3. The larger green balls represent Li^{1+}/Nb^{5+} ions, while the smaller black balls represent O^{2-}/F^{-} ions. In this structure, oxygen octahedrons were formed by a Li^{1+}/Nb^{5+} ion and six O^{2-}/F^{-} ions. The coordination numbers of Li^{1+}/Nb^{5+} and O^{2-}/F^{-} are both six.

The relative densities (ρ_{re}) and apparent densities (ρ_{ap}) of the Li_4NbO_4F ceramics with an increase in the sintering temperature are shown in Fig. 4 ρ_{re} was calculated according to equations (2) and (3):

$$\rho_{th} = \frac{ZM}{NV}, \tag{2}$$

$$\rho_{re} = \frac{\rho_{ap}}{\rho_{th}} \times 100\%, \tag{3}$$

where ρ_{th} is the theoretical density, V is the calculated unit cell volume, M is the molecular weight, Z is the molecule number in a unit cell ($Z = 2$), N is Avogadro's constant, and ρ_{ap} is the measured apparent density. As the sintering temperature increased, both ρ_{ap} and ρ_{re} increased and reached their maximum values at 850 °C (i.e., 3.72 g/cm^3 and 97.0%, respectively). However, when sintered at a higher temperature of

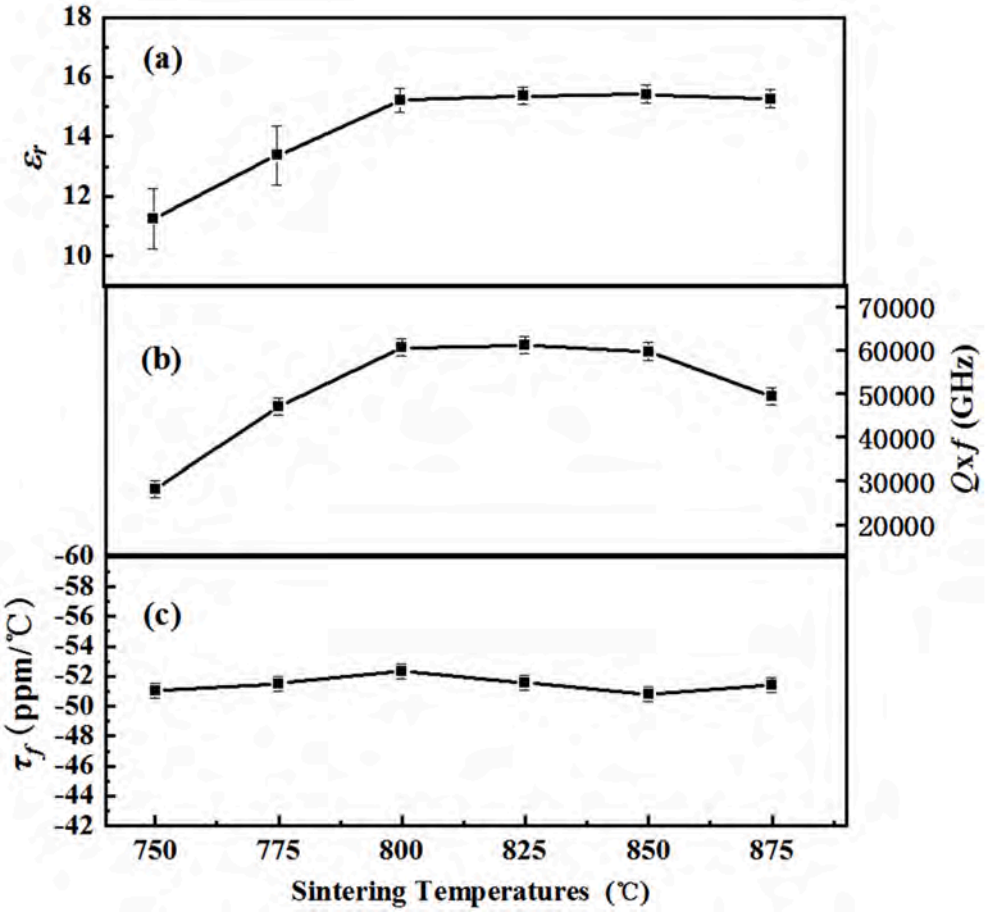

Fig. 6. MDPs of Li_4NbO_4F specimens sintered at various temperatures: (a) ε_r, (b) $Q \times f$, and (c) τ_f.

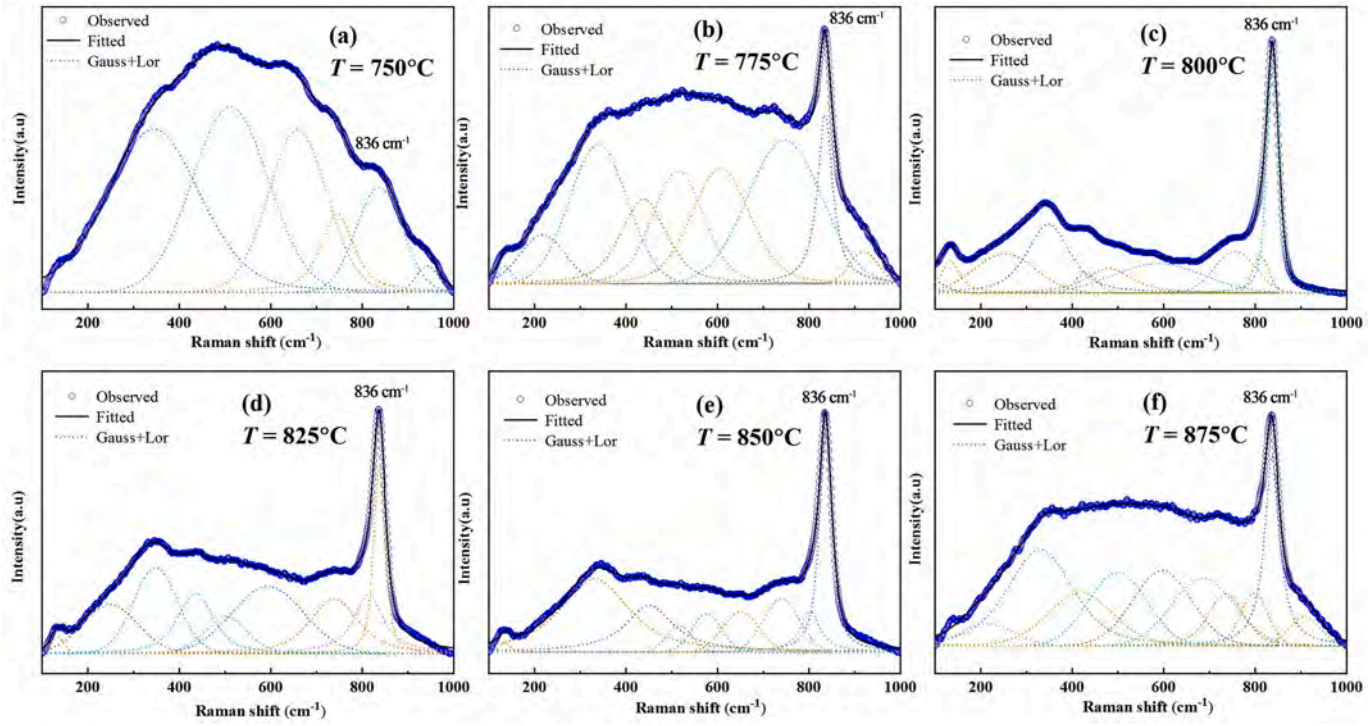

Fig. 7. Raman spectra of Li_4NbO_4F ceramic samples sintered at various temperatures fitted by the Gaussian-Lorentzian function.

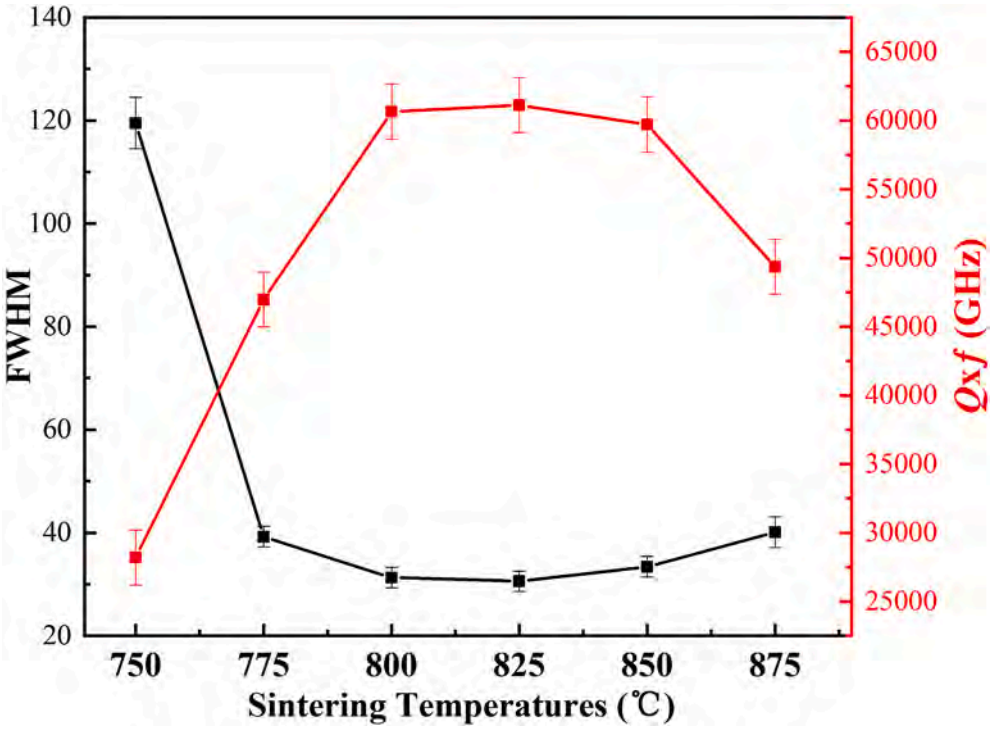

Fig. 8. FWHMs and $Q \times f$ levels of Li_4NbO_4F ceramic samples sintered at various temperatures.

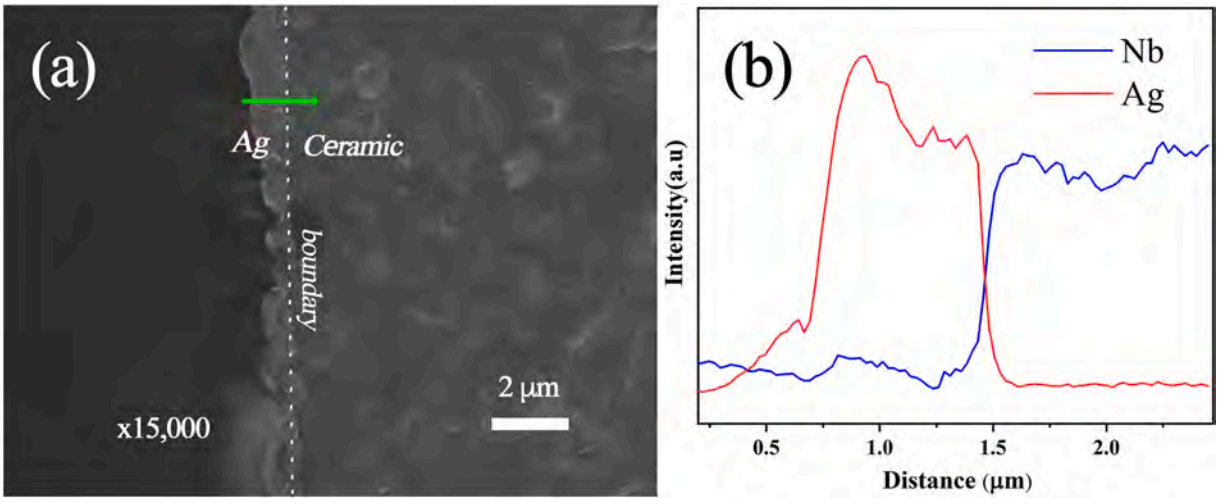

Fig. 9. (a) SEM image of a cross-section view of Li_4NbO_4F sample co-fired with silver at 825 °C and (b) corresponding EDS line-scan results.

875 °C, the densities slightly decreased. This decrease is observed because of the following reasons: (i) a higher sintering temperature accelerated the evaporation of some components (e.g., Li and F), and (ii) abnormal grain growth occurred at 875 °C (as shown later; Fig. 5), which typically leads to a decrease in density. It should be noted that high ρ_{re} (e.g., >96%) was achieved in the Li_4NbO_4F ceramic materials at the sintering temperature of only ~825 °C, which is considerably lower than the sintering temperatures of other previously reported rock-salt-structured ceramic materials (i.e., ~1200 °C) [20,21].

Fig. 5 presents the SEM images of the Li_4NbO_4F ceramics. The insets show the average grain size and grain size distribution of each sample. Relatively high porosity levels were observed in the specimens sintered at 750 and 775 °C, while the samples sintered at higher temperatures exhibited relatively dense microstructures. This is consistent with the results of the density measurements (Fig. 4). Furthermore, as the sintering temperature increased from 750 to 875 °C, the grain size of the specimens increased significantly from 2.12 to 6.96 μm. All samples presented homogeneous microstructures except the one sintered at 875 °C, in which abnormal grain growth was observed.

The MDPs of the Li_4NbO_4F ceramics are illustrated in Fig. 6. With an increase in the sintering temperature from 750 to 800 °C, ε_r of the ceramic samples exhibited a marked increase from 11.3 to 15.2. With a further increase in the sintering temperature to 850 °C, ε_r only slightly increased to 15.4; while sintering at higher temperatures led to a slight decrease in ε_r. The variation in ε_r of the Li_4NbO_4F ceramic samples was consistent with that of ρ_{re} (see Fig. 4). It is widely known that ε_r of ceramic materials is strongly influenced by ρ_{re} because porosity typically results in a significant decrease in ε_r [22]. Moreover, the $Q \times f$ level of the samples increased, then decreased slightly as the sintering temperature increased, reaching its maximum value (61111 GHz) at 825 °C.

Additionally, τ_f was nearly invariable (at approximately −52 ppm/°C) as the sintering temperature varied.

The $Q \times f$ value is known to be dependent on both the extrinsic and intrinsic loss of dielectrics. The extrinsic loss is influenced by factors that mainly include residual porosity and presence of an impurity phase and structural defects [23,24]. In this work, it was found that the $Q \times f$ level increased as ρ_{re} increased, while it decreased as abnormal grain growth occurred. Undoubtedly, these phenomena can be partially ascribed to the microstructural effects on the extrinsic loss in the Li_4NbO_4F ceramic samples. However, the effects of the intrinsic loss are still unclear, and are considered to be dominated by the lattice vibration modes of the materials. Therefore, Raman spectroscopy was performed to study the variation of the lattice vibration modes of the ceramic samples [25,26]. Fig. 7 shows the room temperature Raman spectra of the samples sintered at various temperatures. The Gaussian-Lorentzian model was used to fit the spectra [27]. A strong Raman peak centered at 836 cm^{-1} was observed in each sample, which could be attributed to the symmetric stretching of the NbO_6 octahedra (A_{1g} vibration) [28,29]. Fig. 8 shows the full width at half maximum (FWHM) and $Q \times f$ values of the Li_4NbO_4F samples sintered at various temperatures. For the Raman spectra, their FWHM values usually imply the degree of cation ordering, which has a significant influence on the $Q \times f$ value of MDCMs [30]. A lower FWHM value indicates a higher degree of cation ordering, which can effectively suppress the intrinsic loss and improve the $Q \times f$ level [31]. Fig. 8 shows that the FWHM of the samples decreased as the sintering temperature increased up to 825 °C, above which the FWHM increased. This variation of the FWHM is identical to that of the $Q \times f$ value, implying that, in addition to the above-mentioned microstructural effects, the degree of cation ordering also had a significant effect on the $Q \times f$ value of the Li_4NbO_4F ceramic samples. As a result, the ceramic sample sintered at 825 °C exhibited the highest $Q \times f$ level, because it possessed high density, a homogeneous microstructure, and the highest degree of cation ordering.

For application as an LTCC material, MDCMs must have outstanding chemical compatibility with Ag. A Li_4NbO_4F ceramic sample was co-fired with the Ag electrode at 825 °C. The cross-sectional SEM image and corresponding EDS line-scan results are shown in Fig. 9. A clear boundary between the Ag layer and the ceramic matrix was observed, without apparent Ag diffusion or the formation of a reaction layer. This indicates that, during the sintering process, no apparent chemical reaction between the electrode and the ceramic occurred. Thus, the Li_4NbO_4F ceramic is a promising LTCC material, which has a low sintering temperature, a high $Q \times f$ level, and excellent compatibility with Ag. Considering that the Li_4NbO_4F material possesses a relatively high negative τ_f, further study can focus on strategies to optimize τ_f to a near-zero level.

4. Conclusion

A new rock-salt-structured Li_4NbO_4F ceramic material was fabricated by the solid-state reaction method. Taking advantage of the incorporation of F^- ions into the lattice, this rock-salt-structured material was successfully prepared by low-temperature sintering. The ceramic samples showed high $Q \times f$ levels, which are strongly dependent on the sintering temperature. The highest $Q \times f$ level (i.e., 61111 GHz) was realized in the specimen sintered at 825 °C, because this sample possessed a high density, a homogeneous microstructure, and the highest degree of cation ordering. Moreover, the Li_4NbO_4F ceramic material showed excellent compatibility with Ag. Therefore, the results indicate that Li_4NbO_4F ceramics are promising LTCC materials.

Declaration of competing interest

The authors declare that they have no known competing financial interests or personal relationships that could have appeared to influence the work reported in this paper.

Acknowledgments

This work was supported by the National Science Foundation of China (Nos. 11774083 and 51902093).

References

[1] I.M. Reane, D. Iddles, Microwave dielectric ceramics for resonators and filters in mobile phone networks, J. Am. Ceram. Soc. 89 (2006) 2063–2072.
[2] M. Valant, D. Suvorov, Glass-free low-temperature cofired ceramics: calcium germanates, silicates and tellurates, J. Eur. Ceram. Soc. 24 (2004) 1715–1719.
[3] D. Zhou, D. Guo, W.B. Li, L.X. Pang, X. Yao, D.W. Wang, I.M. Reaney, Novel temperature stable high-: ε r microwave dielectrics in the Bi_2O_3-TiO_2-V_2O_5 system, J. Mater. Chem. C. 4 (2016) 5357–5362.
[4] D. Zhou, L.X. Pang, J. Guo, Z.M. Qi, T. Shao, Q.P. Wang, H.D. Xie, X. Yao, C. A. Randall, Influence of Ce substitution for Bi in $BiVO_4$ and the impact on the phase evolution and microwave dielectric properties, Inorg. Chem. 53 (2014) 1048–1055.
[5] M.T. Sebastian, H. Jantunen, Low loss dielectric materials for LTCC applications: a review, Int. Mater. Rev. 53 (2008) 57–90.
[6] C.F. Tseng, P.J. Tseng, C.M. Chang, Y.C. Kao, Novel temperature stable Li_2MnO_3 dielectric ceramics with high q for LTCC applications, J. Am. Ceram. Soc. 97 (2014) 1918–1922.
[7] Y.H. Zhang, Q.Q. Liu, H.T. Wu, Low-temperature sintering and microwave dielectric properties of H_3BO_3-doped $Li_2Mg_3Ti_{0.95}(Mg_{1/3}Nb_{2/3})_{0.05}O_6$ ceramics, Ceram. Int. 44 (2018) 17526–17529.
[8] C. Li, H. Xiang, C. Yin, Y. Tang, Y. Li, L. Fang, Ultra-low loss microwave dielectric ceramic $Li_2Mg_2TiO_5$ and low-temperature firing via B_2O_3 addition, J. Electron. Mater. 47 (2018) 6383–6389.
[9] P. Zhang, H. Xie, Y. Zhao, X. Zhao, M. Xiao, Low temperature sintering and microwave dielectric properties of $Li_3Mg_2NbO_6$ceramics doped with Li_2O–B_2O_3–SiO_2glass, J. Alloys Compd. 690 (2017) 688–691.
[10] C.-F. Tseng, P.-A. Lin, Microwave dielectric properties of novel glass-free low-firing Li_2CeO_3 ceramics, J. Am. Ceram. Soc. 97 (2014) 1020–1022.
[11] G. Shu, F. Yang, L. Hao, Q. Zhang, F. Meng, H. Lin, Low-firing and microwave dielectric properties of a novel glass-free-MoO_3-based dielectric ceramic for LTCC applications, J. Mater. Sci. Mater. Electron. 30 (2019) 7485–7489.
[12] S. Wang, Y. Ding, M. Wu, Y. Zhang, Effects of ZBS glass addition on sintering behavior and properties of $Ba_{6-3x}(Sm_{1-y}Bi_y)_{8+2x}Ti_{18}O_{54}$(x=2/3, y=0.1) microwave dielectric ceramics, J. Mater. Sci. Mater. Electron. 30 (2019) 11475–11481.
[13] L.L. Yuan, J.J. Bian, Microwave dielectric properties of the lithium containing compounds with rock salt structure, Ferroelectrics 387 (2009) 123–129.
[14] R. Zuo, H. Qi, F. Qin, Q. Dai, A new Li-based ceramic of $Li_4MgSn_2O_7$: synthesis, phase evolution and microwave dielectric properties, J. Eur. Ceram. Soc. 38 (2018) 5442–5447.
[15] J. Bi, Y. Niu, H. Wu, $Li_4Mg_3Ti_2O_9$: a novel low-loss microwave dielectric ceramic for LTCC applications, Ceram. Int. 43 (2017) 7522–7530.
[16] H.L. Pan, H.T. Wu, Crystal structure, infrared spectra and microwave dielectric properties of new ultra low-loss $Li_6Mg_7Ti_3O_{16}$ ceramics, Ceram. Int. 43 (2017) 14484–14487.
[17] Z. Zhang, Y. Tang, H. Xiang, A. Yang, Y. Wang, C. Yin, Y. Tian, L. Fang, $Li_5Ti_2O_6F$: a new low-loss oxyfluoride microwave dielectric ceramic for LTCC applications, J. Mater. Sci. 55 (2020) 107–115.
[18] Z. Zhang, L. Fang, H. Xiang, M. Xu, Y. Tang, H. Jantunen, C. Li, Structural, infrared reflectivity spectra and microwave dielectric properties of the $Li_7Ti_3O_9F$ ceramic, Ceram. Int. 45 (2019) 10163–10169.
[19] P. Zhang, M. Yang, M. Xiao, Z. Zheng, Sintering behavior and microwave dielectric properties of $Li_2Mg_3Ti(O_{1-x/2}F_x)_6$ ($0.06 \le x \le 0.15$) ceramics for LTCC application, Mater. Chem. Phys. 236 (2019), 121805.
[20] X. Chu, L. Gan, S. Ren, J. Wang, Z. Ma, J. Jiang, T. Zhang, Low-loss and temperature-stable $(1-x)Li_2TiO_3$–$xLi_3Mg_2NbO_6$ microwave dielectric ceramics, Ceram. Int. 46 (2020) 8413–8419.
[21] Z. Fu, P. Liu, J. Ma, X. Chen, H. Zhang, New high Q low-fired $Li_2Mg_3TiO_6$ microwave dielectric ceramics with rock salt structure, Mater. Lett. 164 (2016) 436–439.
[22] S.D. Ramarao, V.R.K. Murthy, Structural, Raman spectroscopic and microwave dielectric studies on $Ni_{1-x}(Zn_{1/2}Zr_{1/2})_xW_{1-x}Nb_xO_4$ ceramic compounds with wolframite structure, Dalton Trans. 44 (2015) 2311–2324.
[23] X.H. Ma, S.H. Kweon, S. Nahm, C.Y. Kang, S.J. Yoon, Y.S. Kim, Synthesis and microwave dielectric properties of $Bi_2Ge_3O_9$ ceramics for application as advanced ceramic substrate, J. Eur. Ceram. Soc. 37 (2017) 605–610.
[24] H. Wu, E.S. Kim, Correlations between crystal structure and dielectric properties of high-: Q materials in rock-salt structure Li2O-MgO-BO_2(B = Ti, Sn, Zr)systems at microwave frequency, RSC Adv. 6 (2016) 47443–47453.
[25] H. Zhang, C. Diao, S. Liu, S. Jiang, X. Jing, F. Shi, XRD and Raman study on crystal structures and dielectric properties of $Ba[Mg_{(1-x)/3}Zr_xNb_{2(1-x)/3}]O_3$ solid solutions, Ceram. Int. 40 (2014) 2427–2434.
[26] A. Kan, H. Okazaki, H. Ogawa, Cation ordering and microwave dielectric properties of a $LiGaTiO_4$ spinel by quenching, Jpn. J. Appl. Phys. 58 (2019), SLLE01.
[27] G. Santosh Babu, V. Subramanian, V.R.K. Murthy, R.L. Moreira, R.P.S.M. Lobo, Crystal structure, Raman spectroscopy, far-infrared, and microwave dielectric

properties of (1−x)La(MgSn)$_{0.5}$O$_{3-x}$Nd(MgSn)$_{0.5}$O$_3$ system, J. Appl. Phys. 103 (2008), 084104.

[28] K. Fukumi, S. Sakka, Coordination state of Nb^{5+} ions in silicate and gallate glasses as studied by Raman spectroscopy, J. Mater. Sci. 23 (1988) 2819–2823.

[29] J. Bian, Z. Liang, L. Wang, Structural evolution and microwave dielectric properties of $Li_{(3-3x)}M_{4x}Nb_{(1-x)}O_4$ (M=Mg,Zn; 0≤x≤0.9), J. Am. Ceram. Soc. 94 (2011) 1447–1453.

[30] Z. Xiong, B. Tang, Z. Fang, C. Yang, S. Zhang, Effects of $(Cr_{0.5}Ta_{0.5})^{4+}$ on structure and microwave dielectric properties of $Ca_{0.61}Nd_{0.26}TiO_3$ ceramics, Ceram. Int. 44 (2018) 7771–7779.

[31] J.J. Bian, Y.F. Dong, New high Q microwave dielectric ceramics with rock salt structures: (1-x)Li_2TiO_3 + xMgO system ($0 \leq x \leq 0.5$), J. Eur. Ceram. Soc. 30 (2010) 325–330.